DOI: 10.31276/VJSTE.66(1).24-33

Study on the equilibrium and kinetics of nickel (II) adsorption on cellulose from peanut shell modified with chitosan

Thi Lan Phung*, Thi Kim Giang Nguyen, Phuong Hien Ho, Thanh Nga Pham

Faculty of Chemistry, Hanoi National University of Education, 136 Xuan Thuy Street, Dich Vong Hau Ward, Cau Giay District, Hanoi, Vietnam

Received 12 December 2022; revised 8 March 2023; accepted 20 March 2023

Abstract:

In this study, cellulose was produced by activating peanut shells with 5% NaOH as an alkaline agent and bleaching with 5 wt.% H_2O_2. Before being modified with chitosan, the cellulose was slightly oxidized with ammonium persulfate to introduce carboxyl groups. The equilibrium and kinetics of nickel adsorption on the as-prepared material were investigated. Langmuir, Freundlich, and Temkin isotherm models were used to describe the equilibrium isotherms. The Langmuir and Temkin adsorption isotherms were better fits to the equilibrium data than the Freundlich equation. The Langmuir monolayer adsorption capacity of nickel ions on cellulose from peanut shells modified with chitosan was found to be 25.70 mg/g. The Temkin adsorption constant was calculated as 0.45 kJ/mol. Therefore, the interaction between nickel ions and the surface of the as-prepared material are assumed to be weak. Kinetic data were evaluated by pseudo-first-order and pseudo-second-order models, and rate constants were determined. Simulations demonstrated that the pseudo-second-order equation could adequately describe the adsorption of nickel ions.

Keywords: **adsorption, cellulose, chitosan, isotherms, kinetics, peanut shell.**

Classification numbers: **2.2, 2.3**

1. Introduction

The presence of heavy metal ions such as lead, nickel, cadmium, chromium, arsenic, etc. in industrial effluents poses a significant threat to human health and the environment [1]. These ions easily accumulate in living organisms through the food chain and cause various diseases and metabolic disorders because of their high toxicity and non-degradability in the ecosystem [2, 3]. However, their use cannot be avoided because of their necessity in industries such as tanneries, batteries, electronics, dyeing, textile mills, etc. [4].

Various methods are used to remove heavy metal ions from industrial effluents, such as precipitation, membrane filtration, ion-exchange processes, reverse osmosis methods, and adsorption. Among these methods, adsorption is considered a simple and effective treatment method. Many adsorbents have been successfully studied for heavy metal ion adsorption, such as activated carbon [5], activated agricultural waste materials [6], and biopolymer materials such as cellulose [7] and chitosan [8], whether natural or modified, due to their high mechanical strength, chemical stability, large adsorption capacity, abundance of synthetic materials, low cost, and high reversibility.

In recent years, there has been a trend of using low-cost, highly biodegradable agricultural waste materials [6] such as rice husks, peanut shells, fruit shells, sawdust, bagasse, etc. to limit the emission of agricultural waste after harvest. Peanut shells are one of the most abundant agricultural by-products in Vietnam. The main chemical components of peanut shells include cellulose (40-45%), hemicellulose (<14%), lignin (26-28%), and other components. Therefore, extracting cellulose from peanut shells is also quite attractive [9, 10].

Cellulose is a biodegradable natural polymer composed of thousands of D-glucose units linked β-(1→4) with hydrogen bonding between parallel chains. Cellulose contains many mobile hydroxyl functional groups that easily combine with heavy metal ions and organic pigments [8, 9]. Similarly, chitosan, a linear polysaccharide containing many β -(1-4) D-glucosamine units, possesses both amine and hydroxyl functional

*Corresponding author: Email: lanpt@hnue.edu.vn

groups. These functional groups act as the main complexing agents with metal cations and other agents, making chitosan have a high adsorption capacity for heavy metal ions [11, 12]. Additionally, chitosan is a biodegradable polymer and is also considered as a good candidate to modify cellulose [13, 14].

Prior to modification, cellulose can be partly oxidized from the hydroxyl functional group, such as the CH_2-OH group in the cellulose structure, to the carboxyl functional group to improve its ability to bind with modifying agents. TEMPO and ammonium persulfate are two oxidizing agents frequently used for the mild oxidation of cellulose to introduce carboxyl functional groups on the surface of cellulose. Ammonium persulfate is a cost-effective and environmentally friendly oxidizing agent because of its nontoxicity and mild oxidation conditions. The bond of –O–O– in ammonium persulfate is unstable and readily decomposed into hydrogen peroxide (H_2O_2) and a radical (SO_4^{-*}), which has a strong oxidizing capacity to produce cellulose containing carboxyl groups directly from the raw materials of cellulose [15-17]. The mild oxidation of the CH_2OH group to the COOH group in the cellulose structure increases the association with denaturing agents to increase the adsorption properties and durability of cellulose.

For cellulose/chitosan material, cellulose combines with chitosan through hydrogen bonding between hydroxyl groups of cellulose and chitosan, as well as the electrostatic interaction between the negatively charged carboxylic group of the cellulose matrix and the positively protonated amine of the chitosan solution in acetic acid [16, 18].

This study presents the nickel adsorption capacity of chitosan-modified cellulose material. Cellulose is prepared from peanut shells by alkaline hydrolysis to completely remove lignin, bleached with H_2O_2, and then mild oxidized by ammonium persulfate agent to introduce carboxylic groups, and finally modified with chitosan under suitable experimental conditions. Peanut shells are lignocellulosic materials composed of cellulose (44.8%), hemicellulose (5.6%), and lignin (36.1%) with a complex fibrous structure. The nickel adsorption capacity of chitosan-modified cellulose material was evaluated by changing the contact time and pH of the solution. Additionally, isothermal adsorption models and kinetic models were investigated.

2. Materials and methods

2.1. Chemicals

Nickel sulphate salt ($NiSO_4.6H_2O$), dimethylglyoxime ($C_4H_8N_2O_2$), chitosan, ammonium persulfate ($(NH_4)_2S_2O_8$), sodium hydroxide (NaOH solid and NaOH 0.02 N), acid acetic (CH_3COOH), sodium hydrogen carbonate ($NaHCO_3$ 0.02 N), and hydrochloric acid (HCl) possessed greater than 98% purity and were imported from China. Peanut shells were provided from the region of North Vietnam.

2.2. Preparation of adsorbent

Peanut shells were crushed to sizes in the range of 0.1-0.2 mm. Peanut shell powders were hydrolysed in an alkaline solution with 5% sodium hydroxide solution and bleached with 5% hydrogen peroxide solution to completely remove lignin. Next, the solid was mildly oxidized by ammonium persulfate with a ratio of 1 g/50 ml (peanut shell (g)/ammonium persulfate solution 0.1 M (ml)), by mechanically stirring for 5 h at a temperature of 70°C (denoted as APS-VL) [16, 17]. Finally, the APS-VL sample (2 g) was modified with chitosan solution by impregnation. The chitosan solution was prepared by dissolving 0.35 g of chitosan in 60 ml of 1% acetic acid and mechanically stirred for 3 h. The modifying ratio was equal to 15 wt.% chitosan. The obtained sample was denoted as CTS-APS-VL. The impregnation method was carried out three times. After each impregnation, the CTS-APS-VL sample was dried at 60°C for 4 h. Then, the temperature was raised to 100°C for 3 h to increase the interaction between the surface functional groups of chitosan and the APS-VL sample.

2.3. Characterisation of adsorbent

Amounts of functional groups: The amounts of hydroxyl and carboxyl functional groups on the surface of the APS-VL and CTS-APS-VL samples were determined by Boehm titration. The Boehm agents used were 0.02 N NaOH solution to determine amount of hydroxyl functional group and 0.02 N $NaHCO_3$ solution to determine amount of carboxyl functional group.

Briefly, 0.5 g of adsorbent was added to 50 ml of Boehm agents and then mechanically stirred (150 rpm) for 24 h at room temperature. After the neutral reaction, the solutions were titrated with standardized aqueous HCl (0.02 M) until the end point of phenolphthalein. For 10

ml of solution titrated with 0.02 M HCl, the concentration of hydroxyl and carboxyl functional groups can be calculated as follows, respectively:

$$m_{hydroxyl}(mmol.g^{-1}) = \frac{C_{HCl} \times V^{01}_{HCl} - 5C_{HCl} \times V^{1}_{HCl}}{m} \quad (1)$$

$$m_{carboxyl}(mmol.g^{-1}) = \frac{C_{HCl} \times V^{02}_{HCl} - 5C_{HCl} \times V^{2}_{HCl}}{m} \quad (2)$$

where V^{01}_{HCl}, V^{1}_{HCl} are the volumes of 0.02 HCl used to titrate 50 ml of the initial NaOH solution before the neutralization reaction and 10 ml of the NaOH solution after the neutralization reaction, respectively; C_{HCl} is the concentration of HCl solution. Also; V^{02}_{HCl} and V^{2}_{HCl} are the volumes of 0.02 HCl used to titrate 50 ml of the initial $NaHCO_3$ solution before the neutralization reaction and 10 ml of the $NaHCO_3$ solution after the neutralization reaction, respectively.

Point of zero charge (PZC): Eight solutions of 0.1 M NaCl with different initial pH_i values in the range of 3 and 11 were prepared by adjusting the pH of the solutions using 0.1 M HCl and NaOH. A 0.1-g dosage of the CTS-VL-APS sample was added to 50.0 ml of the 0.1 M NaCl solutions with different initial pH_i values and mechanically stirred (150 rpm) for 24 h at room temperature. Then, the equilibrium pH_j values were measured using a pH meter to calculate the pH_{PZC} value.

EDX analysis: The CTS-APS-VL sample loaded with nickel ions was analysed on an SEM-EDX spectrometer (UV 2600 Shimadzu Instruments) and X-flash 6100 detector to detect the presence of nickel on the surface of the as-prepared sample.

2.4. Methods

The nickel adsorption process was carried out through batch adsorption studies at room temperature. Briefly, 0.4 g of adsorbent was added to 200 ml of nickel solution at a suitable concentration and pH value. After adsorption, the nickel solution was removed to determine the remaining concentration by UV-Vis absorption spectroscopy. The contact time (*t*) was varied from 10 to 140 min. The effect of pH value of the nickel solution was measured from 3.2 to 8.0. The pH value of the nickel solution must be lower than pH 8.0 to avoid the formation of hydrolysed species and precipitation. Additionally, the initial concentration of nickel solutions was changed from 20 to 120 ppm. All other conditions unrelated to the present survey remained constant.

The UV-vis absorption spectra and the standard curve of the complex between nickel solution and dimethylglyoxime at 470 nm are displayed in Figs. 1 and 2, respectively.

Metal ions adsorption capacity of the adsorbents at equilibration time (q_e) and at arbitrary time t (q_t) was calculated according to the following equations:

Adsorption capacity at equilibrium q_e (mg/g):

$$q_e = \frac{(C_o - C_e)xV}{m} \quad (3)$$

Adsorption capacity at arbitrary time t, q_t (mg/g):

$$q_t = \frac{(C_o - C_t)xV}{m} \quad (4)$$

where C_o, C_e, and C_t (ppm) are the concentrations of heavy metal solution at initial time, equilibrium time,

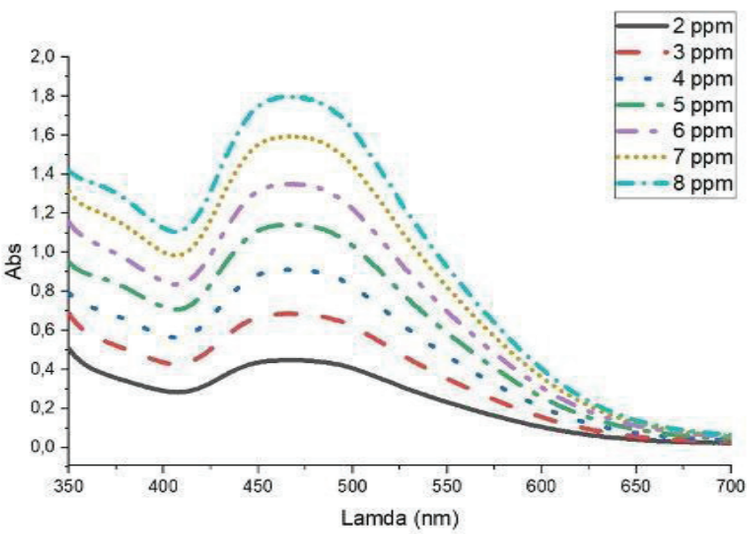

Fig. 1. UV-vis absorption spectrum of the complex between nickel and dimethylglyoxime at 470 nm.

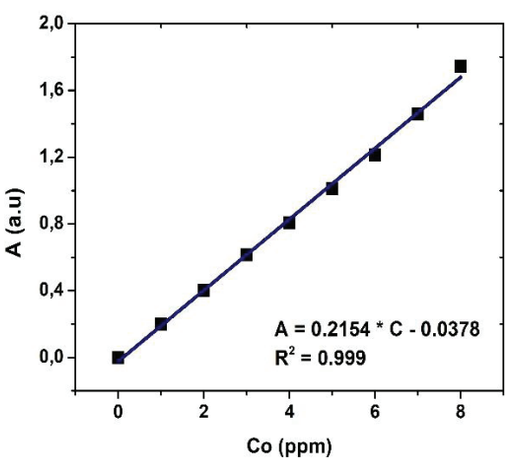

Fig. 2. Standard curve equation of the complex between nickel and dimethylglyoxime at 470 nm.

and contact time, respectively. V is the volume (L) of the heavy metal solution and m is the mass (g) of the adsorbents.

Adsorption Kinetics: Pseudo-first-order and pseudo-second-order models in linearized form were applied to the adsorption kinetic data as follows [19-20]: Pseudo-first-order model in linearised form:

$$\ln(q_{e1} - q_t) = \ln q_{e1} - k_1.t \quad (5)$$

Pseudo-second-order model in linearised form:

$$\frac{t}{q} = \frac{t}{q_{e2}} + \frac{1}{k_2 q_{e2}^2} \quad (6)$$

where the adsorption capacities for the pseudo-first-order model and pseudo-second-order model at equilibria and time t are denoted by q_{e1}, q_{e2}, and q_t, respectively, while k_1 and k_2 are the pseudo-first-order and pseudo-second-order rate constants, respectively.

Equilibrium isotherm modelling: The most common types of models describing equilibrium isotherms are the Langmuir, Freundlich, and Temkin isotherms [19, 20].

The Langmuir isotherm model in linearized form is expressed as:

$$\frac{C_e}{q_e} = \frac{1}{q_m} C_e + \frac{1}{q_{m*K_L}} \quad (7)$$

where q_m (mg/g) and K_L (l/mg) are the maximum monolayer adsorption capacity and a constant related to the heat of adsorption, respectively.

The Freundlich isotherm model in linear form is expressed as:

$$\log q_e = \log K_F + \frac{1}{n} \log C_e \quad (8)$$

where K_F ((mg/g) (L/mg)$^{(1/n)}$) and n are the Freundlich constants related to bonding energy and deviation in adsorption from linearity, respectively. A linear adsorption process is indicated by n=1, a chemical adsorption process is indicated by n<1, and a physical adsorption process is indicated by n>1.

The Temkin isotherm model in non-linear and expressed as:

$$q_e = B \text{ x } \ln (K_T \text{ x } C_e) \quad (9)$$

where K_T is the Temkin's isotherm equilibrium constant (L/g) and $B = RT/b_T$ in which b_T is the Temkin constant; B is constant (J/mol); R is the ideal gas constant (8.314 mol/K); T is absolute temperature (K).

Error analysis: In this study, both R^2 and were used to evaluate the best fit of the isotherm model to the experimental data. The correlation factor was determined from the graphical plots of the isotherms while the chi-squared test was calculated according to Eq. (10):

$$\chi^2 = \sum_1^n \frac{(q_{e\,exp} - q_{e\,(cal.)})^2}{q_{e\,cal.}} \quad (10)$$

where $q_{e\ exp}$ is the experimental metal concentration at equilibrium; $q_{e\ cal}$ is the calculated metal concentration at equilibrium. The best fit is interpreted as the one with the highest correlation coefficient and lowest chi-squared value.

3. Results and discussion

3.1. Characterisation of adsorbent

Amount of functional groups: Table 1 shows the results of the functional group dosage experiments according to the Boehm titration method.

Table 1. The functional group dosage according to the Boehm titration method.

Sample	Hydroxyl group dosage (mmol/g)	Carboxyl group dosage (mmol/g)
APS-VL	1.41	0.55
CTS-APS-VL	2.15	0.26

From Table 1, the APS-VL sample possessed 1.41 mmol/g of hydroxyl groups, which were determined by neutralising with 0.02 N NaOH solution. The carboxyl group dosage was found to be 0.55 mmol/g, which was determined by neutralizing with 0.02 N $NaHCO_3$ solution. The presence of the carboxyl functional group in the cellulose structure after mild oxidation by ammonium persulfate (APS-VL sample) can be explained by the fact that the bond of –O–O– in ammonium persulfate is unstable and readily decomposes into hydrogen peroxide (H_2O_2) and radicals (e.g., HO^* and SO_4^{-*}). After that, these radicals oxidize the hydroxyl groups at the C-6 position in the cellulose structure into carboxyl groups [15-17].

When cellulose was modified by chitosan at a weight ratio of 15% (CTS-APS-VL), the hydroxyl groups in the CTS-APS-VL sample increased to 2.15 mmol/g. This increase could be due to the presence hydroxyl functional groups in the structure of chitosan. However, the carboxyl groups in the CTS-APS-VL sample slightly decreased to 0.26 mmol/g due to the combination of a portion of the carboxyl groups on the surface of cellulose with the amine functional groups on chitosan via the electrostatic interaction between the negatively charged

surfaces of carboxylic groups in the cellulose matrix and the positively protonated amines in the chitosan solution in acetic acid [16, 18]. It is known that the hydroxyl and carboxyl functional groups in the adsorbent may donate protons and become deprotonated groups (C-O^- and COO^-), which are involved in coordination with nickel ions, resulting in an increase in the adsorption of the nickel ions [21].

Point of zero charge (PZC): The point of zero charge (PZC) parameter is used to assess the surface properties of an adsorbent. The pH of the solution required to yield a net zero surface charge is denoted by pH_{PZC}. Therefore, the surface of an adsorbent has a net positive surface charge at $pH<pH_{PZC}$, while it has a net negative surface charge at $pH>pH_{PZC}$. Fig. 3 displays the plot of $H = pH_i - pH_j$ vs pH_i to calculate the pH_{PZC} value.

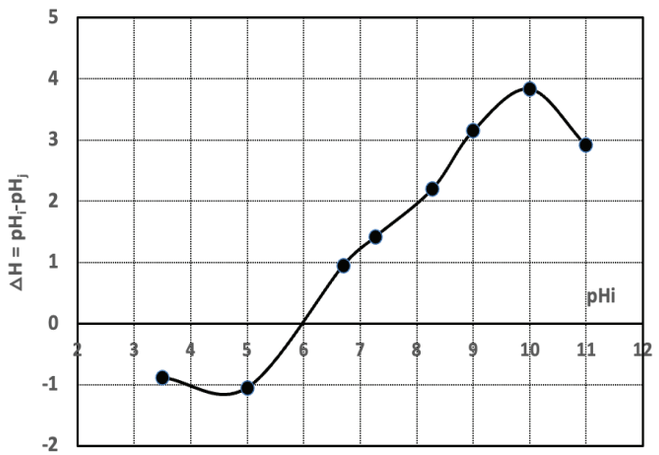

Fig. 3. The plot of $H = pH_i - pH_j$ vs pH_i of the CTS-APS-VL sample.

From Fig. 3, the pH_{PZC} value of the CTS-APS-VL sample was determined to be 6.0. At pH<6 the surface of the material is positively charged due to protonation of the hydroxyl and carboxyl functional groups, while it is negatively charged at pH>6 as a result of deprotonation. At pH>6, the material favours metal cation adsorption. Therefore, the pH_{PZC} value for the CTS-APS-VL sample indicates that the adsorption of nickel ions will occur at pH≥6.0

EDX spectroscopy: The EDX spectroscopy clearly shows that nickel ions are adsorbed onto the chitosan-modified peanut shell (as shown Fig. 4). From EDX analysis, the nickel content was found to be about 5.7 wt.%, indicating the successful adsorption of nickel on cellulose from chitosan-modified peanut shells.

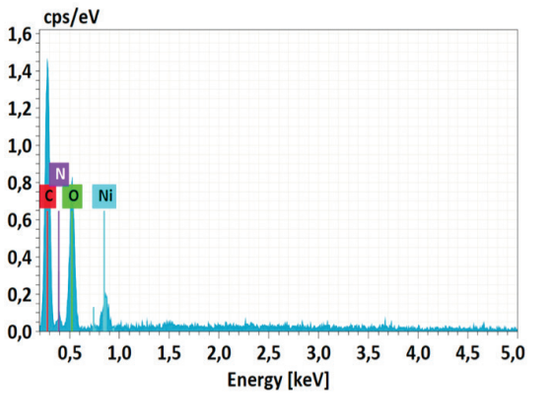

Fig. 4. EDX spectroscopy of CTS-APS-VL loaded with nickel.

3.2. Nickel adsorption capacity of chitosan-modified peanut shell

Figure 5 shows the nickel adsorption capacity of cellulose from chitosan-modified peanut shells at different times.

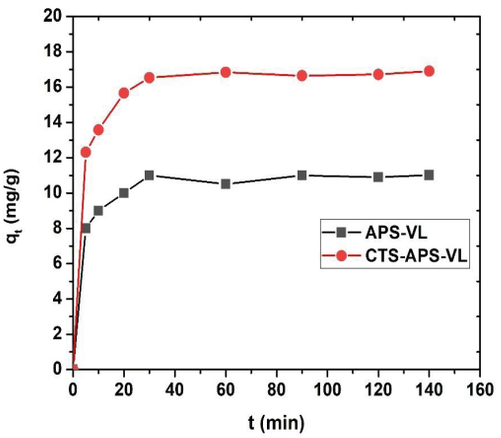

Fig. 5. Nickel adsorption capacity of the APS-VL and CTS-APS-VL samples using 200 ml of nickel solution with an initial concentration of 80 ppm at pH 7.0, and 0.4 g of adsorbent over an adsorption period of 10-140 min.

The experimental data showed that the nickel adsorption capacity increased as the adsorption time increased from 10 to 60 min, and it reached equilibrium after 90 min. In the as-prepared samples, the hydroxyl and carboxyl functional groups played a major role in nickel adsorption. The adsorption of nickel ions on the surface of the as-prepared samples was accomplished through physical processes including both weak electrostatic interaction and Van der Waals forces, or through the formation of complexation between the nickel ion and carboxyl and hydroxyl anion on the surface of as-prepared materials.

The adsorption capacities at equilibrium time (q_e in mg/g) of the APS-VL and CTS-APS-VL samples were found to be 11.10 and 16.90 mg/g, respectively. Therefore, the nickel adsorption capacity of the CTS-APS-VL sample was higher than that of the APS-VL sample. Furthermore, the amount of hydroxyl groups in the CTS-APS-VL sample was higher than that of APS-VL and the amount of carboxyl groups in CTS-APS-VL was lower than that of APS-VL. This result suggests that the presence of hydroxyl groups is the main agent for adsorbing nickel ions onto the CTS-APS-VL sample.

Similar to adsorption time, the pH of the working solution has a strong influence on the adsorption capacity of metal ions by affecting surface charge density of the adsorbent (dissociation of oxygen containing functional groups) and the degree of ionization and state of heavy metal ion species in the solution. In this study, nickel adsorption was investigated in the pH range of 3.2-8.0. The obtained results are depicted in Fig. 6.

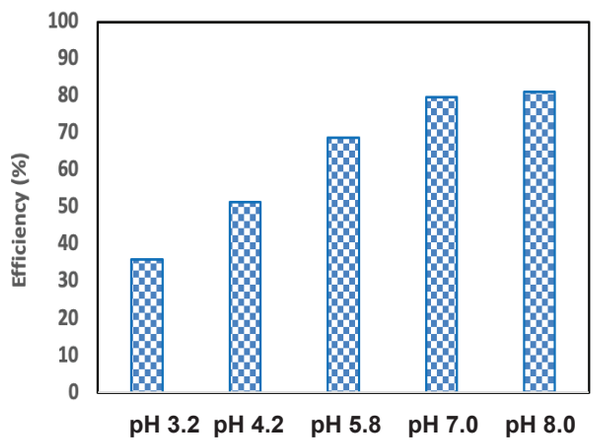

Fig. 6. Effect of pH on the adsorption of nickel (II) onto the CTS-APS-VL sample with 200 ml of nickel solution with an initial concentration of 80 ppm, 0.4 g of adsorbent, and an adsorption time 90 min in pH range of 3.2-8.0.

As depicted in Fig. 6, the nickel adsorption capacity (in terms of percent efficiency) increased with increasing solution pH. A maximum adsorption efficiency of about 81.05% occurred at pH 7.0 and 8.0, and the adsorption capacity at equilibrium time (q_e in mg/g) of the APS-VL sample was 16.90 mg/g. The minimum nickel adsorption efficiency of 35.98% at pH 3.2 may be due to the high concentration and high mobility of H^+ ions. Thus, the hydrogen ions are preferentially adsorbed rather than the metal ions (e.g., nickel ions). At higher pH values, the nickel adsorption efficiency was enhanced because the hydrogen ions were less preferentially adsorbed than the metal ions due to the lower number of H^+. On the other hand, the pH_{PZC} of the CTS-APS-VL sample and different species of nickel ions in the solution could be used to describe how the pH of the solution affects the adsorption capacity of CTA-APS-VL. The point of zero charge (pH_{pzc}) of the CTS-APS-VL sample was determined to be 6.0 (as shown in Fig. 3), and the nickel solution comprises nickel species with different coordination numbers such as Ni^{2+}, $Ni(OH)^+$, and $Ni(OH)_2$ in a pH range of 3.2 to 8.0. These species are adsorbed onto the surface of CTS-APS-VL by an ion exchange mechanism with the functional groups present in CTS-APS-VL or by hydrogen bonding, as shown below:

Ion exchange:

$$2(–ROH) + Ni^{2+} \rightarrow 2(RO)Ni + 2H^+ \; –ROH + Ni(OH)^+ \rightarrow (–RO)\,Ni(OH) + H^+$$

Hydrogen bonding:

$$2(–ROH) + Ni(OH)_2 \rightarrow (–ROH)_2 + Ni(OH)_2$$

where R represents the matrix of CTS-APS-VL.

At a low pH of 3.2, the surface of CTS-APS-VL is positively charged due to protonation of the hydroxyl and carboxyl functional groups and unfavourable conditions for the adsorption of the Ni^{2+} and $Ni(OH)^+$ species. As the pH solution increased, the surface of CTS-APS-VL became less positive and therefore electrostatic attraction between the Ni^{2+} and $Ni(OH)^+$ species and the surface groups likely increased.

In this study, the pH value of each metal ion solution had to be lower than 8 to prevent the formation of hydrolysed species and precipitation. If the pH value exceeds 8, the adsorption mechanism changes, affecting the efficiency of the adsorption.

3.3. Adsorption kinetics

In order to understand the kinetics of nickel adsorption using cellulose from chitosan-modified peanut shells as an adsorbent, pseudo-first-order and pseudo-second-order kinetic models were tested with the experimental data.

Pseudo-first-order model: The pseudo-first-order model in linearized form is expressed in Eq. (3). The rate constant, k_1, was calculated from the slope and intercept of the plot of $\log(q_e\text{-}q_t)$ vs time (as shown in Fig. 7). The equilibrium adsorption capacity (q_e) calculated from Eq. (3) is referred to as the calculated value of equilibrium adsorption capacity ($q_{e(TT)}$).

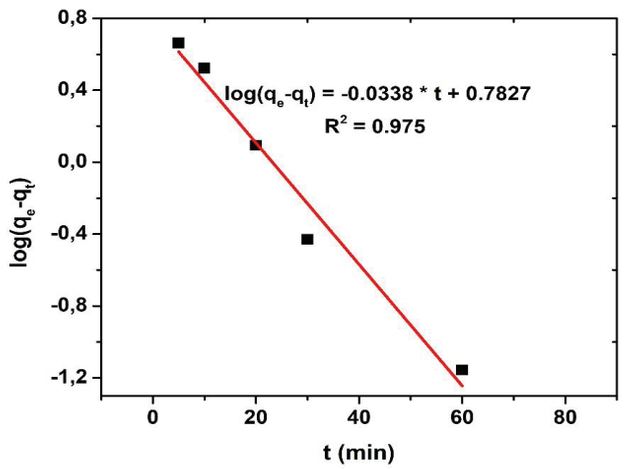

Fig 7. Linear plot of $\log(q_e-q_t)$ vs t of nickel adsorption onto the CTS-APS -VL sample with 200 ml of nickel solution with an initial concentration of 80 ppm, pH 7.0, 0.4 g of adsorbent, and a range of adsorption time of 10-60 min.

As shown in Fig. 7, the rate constant k_1 was determined to be 0.077 min^{-1}. It is also possible to calculate the equilibrium adsorption capacity, which was found to be 6.06 mg/g (denoted $q_{e\ cal}$). In fact, the calculated equilibrium adsorption capacity, q_{ecal}, should be in accordance with the experimental adsorption capacity $q_{e\ exp}$ [19, 20]. Although the correlation coefficient values (R^2) are very high, the calculated ones, obtained from the linear plots (Table 2), did not agree with experiment ($q_{e\ exp}$ =16.90 mg/g). This suggests that nickel adsorption does not follow pseudo-first-order kinetics.

Table 2. Kinetic parameters for nickel adsorption on cellulose from chitosan-modified peanut shells.

Kinetic models	Parameters	
Pseudo-first-order model	k_1 (min^{-1})	0.077
	$q_{e\ cal}$ (mg/g)	6.06
	R^2	0.975
Pseudo-second-order model	k_2 (g/(mg x min)	0.024
	$q_{e\ cal}$ (mg/g)	17.54
	R^2	0.999

Pseudo-second-order model: The nickel adsorption kinetic data can also be described by pseudo-second-order model, which is expressed in Eq. (4).

The pseudo-second-order rate constant, k_2, and $q_{e\ cal}$ values were calculated from the slope and intercept of the plots t/q vs. t (as shown in Fig. 8). The rate constant, k_2, was 0.024 g/(mg.min). The calculated equilibrium adsorption capacity ($q_{e\ cal}$) was 17.54 mg/g. Therefore, the calculated q_e values agreed well with experimental q_e values (Table 2), thus the pseudo-second-order kinetic model well described the nickel adsorption kinetic data.

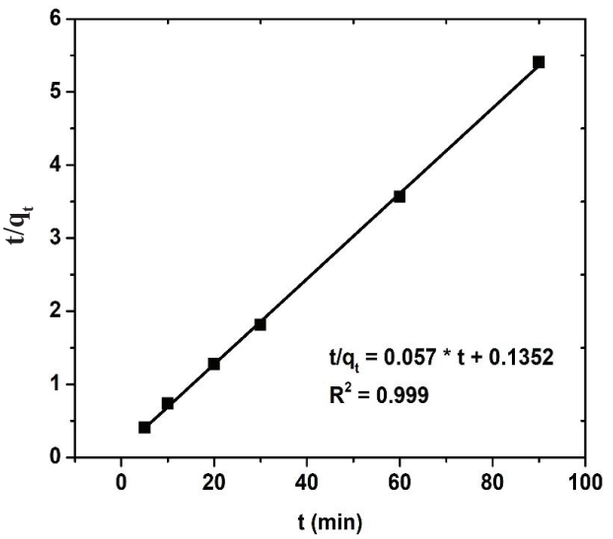

Fig. 8. Linear plot of t/q_t vs t of nickel adsorption onto the CTS-APS-VL sample with 200 ml of nickel solution with an initial concentration of 80 ppm, a pH of 7.0, 0.4 g of adsorbent, and an adsorption period of 10-90 min.

3.4. Adsorption isotherms

Adsorption isotherms indicate how adsorbates interact with adsorbents and how equilibrium is established between adsorbed metal ions on the adsorbent. The maximum adsorption capacity is determined by equilibrium isotherms. The most common types of models are the Langmuir, Freundlich, and Temkin isotherms.

Langmuir isotherm model: The Langmuir isotherm assumes a monolayer of adsorbates covering a homogeneous adsorbent surface. This suggests that once an adsorbate occupies an available adsorption site, no further adsorption can take place at that site. Additionally, the adsorption activation energy is assumed to be equal for each molecule that adsorbs onto the surface.

Figure 9 presents a linear plot of C_e/q_e vs C_e for the experimental adsorption isotherm of nickel ions on chitosan-modified peanut shells at room temperature. The Langmuir isotherm constant and correlation coefficients are given in Table 3, with a maximum monolayer adsorption capacity (q_m) for nickel removal of 25.70 mg/g.

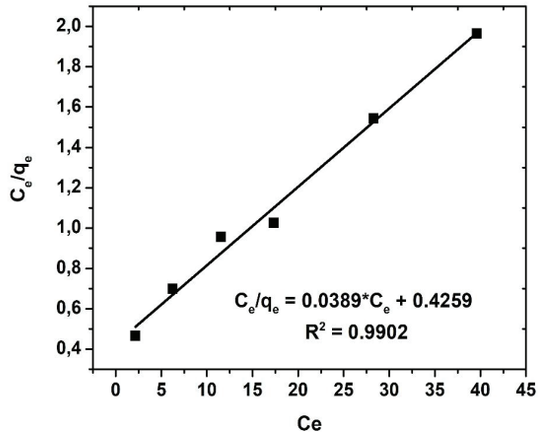

Fig. 9. Linear plot of C_e/q_e vs C_e for nickel adsorption onto the CTS-APS -VL sample with 200 ml of nickel solution over a range of initial concentrations (20-120 ppm), pH of 7.0, equilibrium adsorption time of 90 min, and 0.4 g of adsorbent.

Table 3. Adsorption isotherm parameters.

Isotherm model	Parameters	Non-linear equation
Langmuir model	q_m=25.70 mg/g K_L=0.09 l/mg R^2=0.990 χ^2=0.234	$q_e = \frac{2.34 * C_e}{(1 + 0.09 * C_e}$
Freundlich model	K_F=3.35 n=1.94 R^2=0.974 χ^2=0.632	$q_e = 3.35 * C_e^{0.51}$
Temkin model	b_T=4.52 kJ/mol K_T=0.94 R^2=0.974 χ^2=0.433	$q_e = 5.70 \times \ln(0.45 \times C_e)$

Freundlich isotherm model: Unlike the Langmuir isotherm model, the Freundlich isotherm model assumes that the adsorption process occurs in multilayers, where each adsorption centre can adsorb more than one adsorbed molecule.

Figure 10 shows the linear plot of $\log(q_e)$ vs. $\log(C_e)$ for the experimental adsorption isotherm of nickel ions on the CTS-APS-VL sample at room temperature.

The Freundlich adsorption constants, evaluated from the isotherms, with correlation coefficients and are listed in Table 3.

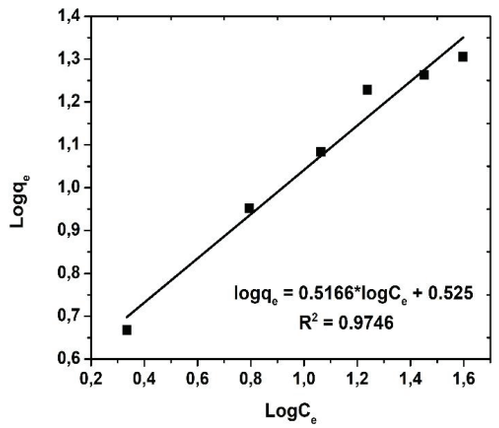

Fig. 10. Linear plot of $\log(q_e)$ vs. $\log(C_e)$ of nickel adsorption onto the CTS-APS-VL sample with 200 ml of nickel solution over a range of initial concentrations of 20-120 ppm, pH 7.0, equilibrium adsorption time of 90 min, and 0.4 g of adsorbent.

Temkin isotherm model: The Temkin isotherm model is concerned with the influence of adsorbent-adsorbent interaction on the adsorption equilibrium. The model assumes that the adsorption heat (as a function of temperature) of all adsorbents in a layer will decrease linearly, rather than logarithmically, with increasing surface coverage.

Figure 11 shows a linear plot of q_e vs $\ln(C_e)$ of the experimental adsorption isotherm of nickel ions on modified peanut shells at room temperature.

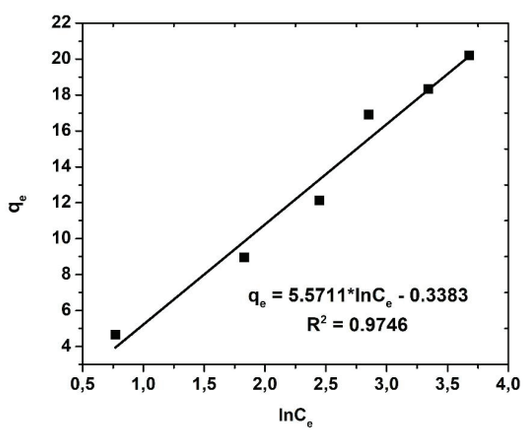

Fig. 11. The linear plot of q_e vs $\ln(C_e)$ onto the CTS-APS-VL sample with 200 ml of nickel solution over a range of initial concentrations of 20-120 ppm, pH 7.0, an equilibrium adsorption time of 90 min, and 0.4 g of adsorbent.

The Temkin adsorption constant was calculated to be 0.45 kJ/mol, which is lower than 8 kJ/mol. Therefore, it can be assumed that the interaction between nickel ions and the surface of the as-prepared adsorbent was weak.

As shown in Table 3, the values of R^2 and indicate that the Langmuir and Temkin isotherm models exhibited a better fit than the Freundlich model for nickel adsorption. The lower the value, the better the fit of the line to the data, and the higher the R^2 value, the better the fit.

Table 4 displays a comparison of the maximum adsorption capacity of nickel onto various modified agro-wastes. CTS-AP-VL was found to have a relatively large adsorption capacity, and this indicates that it is a promising material for the removal of metal ions from aqueous solutions.

Table 4. Comparison of maximum adsorption capacity of nickel onto other agro-wastes.

Materials	Maximum sorption capacity (mg/g)	References
Chemically Treated Mahogany Sawdust	13.42	[21]
Chemically modified orange peel	162.6	[20]
Phthalate-functionalized sugarcane bagasse	53.94	[22]
Na_2CO_3-modified Miller leaf powder	28.98	[23]
HCl modified meranti sawdust	35.97	[24]
CTS-APS-VL	25.70	This study

4. Conclusions

The cellulose isolated from chitosan-modified peanut shells (CTS-APS-VL) showed better adsorption capacity compared to cellulose isolated from peanut shells (APS-VL) under the same experimental conditions. The adsorption capacity at equilibrium time (q_e in mg/g) of the APS-VL and CTS-APS-VL samples were found to be 11.10 and 16.90 mg/g, respectively, at an adsorption time of 90 min, initial nickel concentration of 80 ppm, volume of 200 ml, and adsorbent mass of 0.4 g. The pseudo-second-order kinetics model was better suited to the data than the pseudo-first-order model. The rate constant, k_2, was determined to be 0.024 (g/(mg.min)). The calculated equilibrium adsorption capacity ($q_{e\ cal}$) was 17.54 mg/g. The Langmuir and Temkin isotherm models showed slightly better results than the Freundlich model for the as-prepared material, indicating monolayer coverage. According to the Langmuir model, the maximum monolayer adsorption capacity (q_m) for nickel removal was 25.70 mg/g. The Temkin adsorption constant was calculated as 0.45 kJ/mol and it can be assumed that the interaction between the nickel ions and the surface of the as-prepared adsorbent was weak.

CRediT author statement

Thi Lan Phung: Conceptualisation, Methodology, Formal analysis, Writing, Reviewing, Editing; Thi Kim Giang Nguyen: Data analysis; Phuong Hien Ho: Reviewing, Data analysis; Thanh Nga Pham: Reviewing, Editing.

ACKNOWLEDGEMENTS

The research funding from the Vietnam Ministry of Education and Training under grant code B2021-SPH 14 was acknowledged.

COMPETING INTERESTS

The authors declare that there is no conflict of interest regarding the publication of this article.

REFERENCES

[1] J. Li, X. Wang, G. Zhao, et al. (2018), "Metal-organic framework-based materials: superior adsorbents for the capture of toxic and radioactive metal ions", *Chem. Soc. Rev*., **47(7)**, pp 2322-2356, DOI: 10.1039/C7CS00543A.

[2] W. Ouyang, Y. Wang, C. Lin, et al. (2018), "Heavy metal loss from agricultural watershed to aquatic system: A scientometrics review", *Sci. Total Environ*., **637**, pp.208-220, DOI: 10.1016/j.scitotenv.2018.04.434.

[3] C. Zhu, F. Liu, Y. Zhang, et al. (2016), "Nitrogen-doped chitosan-Fe(III) composite as a dual-functional material for synergistically enhanced co-removal of Cu(II) and Cr(VI) based on adsorption and redox", *Chem. Eng. J*., **306**, pp.579-587, DOI: 10.1016/j.cej.2016.07.096.

[4] K.H. Vardhan, P.S. Kumar, R.C. Panda (2019), "A review on heavy metal pollution, toxicity and remedial measures: Current trends and future perspectives", *J. Mol. Liq*., **290**, DOI: 10.1016/j.molliq.2019.111197.

[5] M.D. Vedenyapina, A.Y. Kurmysheva, S.A. Kulaishin, et al. (2021), "Adsorption of heavy metals on activated carbons: A review", *Solid Fuel Chem*., **55**, pp.83-104, DOI: 10.3103/S0361521921020099.

[6] M. Bilal, I. Ihsanullah, M. Younas, et al. (2022), "Recent advances in applications of low-cost adsorbents for the removal of heavy metals from water: A critical review", *Separation and Purification Technology*, **278**, DOI: 10.1016/j.seppur.2021.119510.

[7] A. Jamshaid, A. Hamid, N. Muhammad, et al. (2017), "Cellulose-based materials for the removal of heavy metals from wastewater - An overview", *Chem. Bio. Eng. Rev.*, **4(4)**, pp.1-18.

[8] E. Khademian, E. Salehi, H. Sanaeepur, et al. (2020), "A systematic review on carbohydrate biopolymers for adsorptive remediation of copper ions from aqueous environments-part A: Classification and modification strategies", *Science of The Total Environment*, **738**, DOI: 10.1002/cben.201700002.

[9] O. Bobet, S. Nassio, M. Seynou, et al. (2020), "Characterization of peanut shells for their valorization in earth brick", *Journal of Minerals and Materials Characterization and Engineering*, **8(4)**, pp.301-315, DOI: 10.4236/jmmce.2020.84018.

[10] P. Ganguly, S. Sengupta, P. Das, et al. (2020), "Synthesis of cellulose from peanut shell waste and its use in bioethanol production", *Bioresource Utilization and Bioprocess Book*, pp.81-91, DOI: 10.1007/978-981-15-1607-8_10.

[11] I. Sargın, G. Arslan (2015), "Chitosan/sporopollenin microcapsules: Preparation, characterisation and application in heavy metal removal", *Int. J. Biol. Macromol*., **75**, pp.230-238, DOI: 10.1016/j.ijbiomac.2015.01.039.

[12] L. Zhang, Y. Zeng, Z. Cheng (2016), "Removal of heavy metal ions using chitosan and modified chitosan: A review", *Journal of Molecular Liquids*, **214**, pp.175-191, DOI: 10.1016/j.molliq.2015.12.013.

[13] M.D.H. Rahaman, A. Islam, M. Islam, et al. (2021), "Biodegradable composite adsorbent of modified cellulose and chitosan to remove heavy metal ions from aqueous solution", *Current Research in Green and Sustainable Chemistry*, **4**, pp.100-119, DOI: 10.1016/j.crgsc.2021.100119.

[14] D. Zhang, L. Wang, H. Zeng, et al. (2019), "A three-dimensional macroporous network structured chitosan/cellulose biocomposite sponge for rapid and selective removal of mercury (II) ions from aqueous solution", *Chemical Engineering Journal*, **363**, pp.192-202, DOI: 10.1016/j.cej.2019.01.127.

[15] K. Zhanga, P. Suna, H. Liua, et al. (2016), "Extraction and comparison of carboxylated cellulose nanocrystals from bleached sugarcane bagasse pulp using two different oxidation methods", *Carbohydrate Polymers*, **138**, pp.237-243, DOI: 10.1016/j.carbpol.2015.11.038.

[16] A.M. Adel, A.M.E. Shafei, M.T.A. Shemy, et al. (2017), "Influence of cellulose polymorphism on tuneable mechanical and barrier properties of chitosan/oxidized nanocellulose bio-composites", *Egypt. J. Chem*., **60(4)**, pp.639-652, DOI: 10.21608/ejchem.2017.1194.1062.

[17] Y. Liu, K. Wang, H. Zhang, et al. (2020), "Modified ammonium persulfate oxidations for efficient preparation of carboxylated cellulose nanocrystals", *Carbohydrate Polymers*, **229**, DOI: 10.1016/j.carbpol.2019.115572.

[18] B. Soni, E.B. Hassan, M.W. Schilling, et al. (2016), "Transparent bionanocomposite films based on chitosan and TEMPO-oxidized cellulose nanofibers with enhanced mechanical and barrier properties", *Carbohydrate Polymers*, **151**, pp.779-789, DOI: 10.1016/j.carbpol.2016.06.022.

[19] J. Febrianto, A.N. Kosasih, J. Sunarso, et al. (2009), "Equilibrium and kinetic studies in adsorption of heavy metals using biosorbent: A summary of recent studies", *J. Hazard. Mater*., **162**, pp.616-645.

[20] N. Feng, X. Guo, S. Liang, et al. (2011), "Biosorption of heavy metals from aqueous solutions by chemically modified orange peel", *Journal of Hazardous Materials*, **185(1)**, pp.49-54, DOI: 10.1016/j.jhazmat.2010.08.114.

[21] R. Chanda, A.H. Mithun, A. Hasan, et al. (2021), "Nickel removal from aqueous solution using chemically treated mahogany sawdust as biosorbent", *Hindawi Journal of Chemistry*, **2021**, DOI: 10.1155/2021/4558271.

[22] S.N.D.C. Ramos, A.L.P. Xavier, F.S. Teodoro, et al. (2016), "Removal of cobalt(II), copper(II), and nickel(II) ions from aqueous solutions using phthalate-functionalized sugarcane bagasse: Monoand multicomponent adsorption in batch mode", *Industrial Crops and Products*, **79**, pp.116-130, DOI: 10.1016/j.indcrop.2015.10.035.

[23] S. Gupta, S.K. Sharma, A. Kumar (2019), "Biosorption of Ni(II) ions from aqueous solution using modified Aloe barbadensis Miller leaf powder", *Water Science and Engineering*, **12(1)**, pp.27-36, DOI: 10.1016/j.wse.2019.04.003.

[24] M. Rafatullaha, O. Sulaiman, R. Hashim, et al. (2009), "Adsorption of copper (II), chromium (III), nickel (II) and lead (II) ions from aqueous solutions by meranti sawdust", *Journal of Hazardous Materials*, **170(2-3)**, pp.969-977, DOI: 10.1016/j.jhazmat.2009.05.066.